

# First discoveries of $z \sim 6$ quasars with the Kilo Degree Survey and VISTA Kilo-Degree Infrared Galaxy survey<sup>\*</sup>

B. P. Venemans,<sup>1†</sup> G. A. Verdoes Kleijn,<sup>2</sup> J. Mwebaze,<sup>2</sup> E. A. Valentijn,<sup>2</sup>  
 E. Bañados,<sup>1</sup> R. Decarli,<sup>1</sup> J. T. A. de Jong,<sup>3</sup> J. R. Findlay,<sup>4</sup> K. H. Kuijken,<sup>3</sup>  
 F. La Barbera,<sup>5</sup> J. P. McFarland,<sup>2</sup> R. G. McMahon,<sup>6,7</sup> N. Napolitano,<sup>5</sup>  
 G. Sikkema<sup>2</sup> and W. J. Sutherland<sup>8</sup>

<sup>1</sup>Max-Planck Institute for Astronomy, Königstuhl 17, D-69117 Heidelberg, Germany

<sup>2</sup>Kapteyn Astronomical Institute, University of Groningen, PO Box 800, NL-9700 AV Groningen, The Netherlands

<sup>3</sup>Leiden Observatory, Leiden University, P.O. Box 9513, NL-2300 RA Leiden, The Netherlands

<sup>4</sup>Department of Physics and Astronomy, University of Wyoming, Laramie, WY 82071, USA

<sup>5</sup>Astronomical Observatory of Capodimonte - INAF, via Moiariello 16, I-80131, Napoli, Italy

<sup>6</sup>Institute of Astronomy, University of Cambridge, Madingley Road, Cambridge CB3 0HA, UK

<sup>7</sup>Kavli Institute for Cosmology, University of Cambridge, Madingley Road, Cambridge CB3 0HA, UK

<sup>8</sup>Astronomy Unit, School of Mathematical Sciences, Queen Mary, University of London, London, E1 4NS, UK

Accepted 2015 July 31. Received 2015 July 31; in original form 2015 June 30

## ABSTRACT

We present the results of our first year of quasar search in the ongoing ESO public Kilo Degree Survey (KiDS) and VISTA Kilo-Degree Infrared Galaxy (VIKING) surveys. These surveys are among the deeper wide-field surveys that can be used to uncover large numbers of  $z \sim 6$  quasars. This allows us to probe a more common population of  $z \sim 6$  quasars that is fainter than the well-studied quasars from the main Sloan Digital Sky Survey. From this first set of combined survey catalogues covering  $\sim 250 \text{ deg}^2$  we selected point sources down to  $Z_{\text{AB}} = 22$  that had a very red  $i - Z$  ( $i - Z > 2.2$ ) colour. After follow-up imaging and spectroscopy, we discovered four new quasars in the redshift range  $5.8 < z < 6.0$ . The absolute magnitudes at a rest-frame wavelength of  $1450 \text{ \AA}$  are between  $-26.6 < M_{1450} < -24.4$ , confirming that we can find quasars fainter than  $M^*$ , which at  $z = 6$  has been estimated to be between  $M^* = -25.1$  and  $M^* = -27.6$ . The discovery of four quasars in  $250 \text{ deg}^2$  of survey data is consistent with predictions based on the  $z \sim 6$  quasar luminosity function. We discuss various ways to push the candidate selection to fainter magnitudes and we expect to find about 30 new quasars down to an absolute magnitude of  $M_{1450} = -24$ . Studying this homogeneously selected faint quasar population will be important to gain insight into the onset of the co-evolution of the black holes and their stellar hosts.

**Key words:** cosmology: observations — galaxies: active — galaxies: quasars: general

## 1 INTRODUCTION

Supermassive black holes (SMBHs) are inferred to reside at the nuclei of most (if not all) massive galaxies. In present day galaxies, tight correlations are observed between the black hole mass and global host parameters over at least three orders of magnitude in black hole mass (see e.g.

Kormendy & Ho 2013, for a recent review). Going back in time, the global history of star formation and of radiative mass accretion on to black holes display similar behaviour as a function of time, peaking at redshifts  $\sim 2 - 3$  (Heckman et al. 2004; for a review see Madau & Dickinson 2014 and references therein). Determining the physical processes that govern the symbiotic relationship between SMBHs and their host galaxies is an outstanding challenge in astrophysics. Studying the SMBHs and stellar hosts of high-redshift ( $z > 5.7$ ) quasars is one of the most direct ways to obtain insight on the onset of this relation in the first Gyr after the big bang. They provide funda-

<sup>\*</sup> Based on observations collected at the European Southern Observatory, Chile, programmes 177.A-3016, 179.A-2004, 089.A-0290, 089.A-0596, 090.A-0383, 090.A-0642 and 091.A-0421.

<sup>†</sup> E-mail: venemans@mpia.de

mental constraints on the formation and growth of the first SMBHs, on early star formation and on chemical enrichment in galaxy hosts and the surrounding intergalactic matter (e.g. Fan et al. 2006; Jiang et al. 2007; De Rosa et al. 2011; Carilli & Walter 2013).

Thanks to large imaging surveys of moderate depth, it has become feasible to identify the rare bright quasars photometrically at high redshifts. As an illustration, a luminous quasar at redshift 6 can be detected photometrically in the  $z$  band within two minutes on a 2.5 m telescope. In the past decade about 70 bright quasars at  $z > 5.7$  have been discovered (e.g. Fan et al. 2006; Jiang et al. 2009; Willott et al. 2010b; Mortlock et al. 2011; Bañados et al. 2014; Venemans et al. 2015) using a variety of different multiwavelength surveys such as the Sloan Digital Sky Survey (SDSS; Abazajian et al. 2009), the Canada-France High- $z$  Quasar Survey (CFHQS; Willott et al. 2010b), the UK Infrared Telescope Infrared Deep Sky Survey (UKIDSS; Lawrence et al. 2007) and Panoramic Survey Telescope & Rapid Response System 1 (Pan-STARRS1; Morganson et al. 2012; Bañados et al. 2014).

These quasars appear to have SMBH masses equivalent to today’s most massive galaxies with high-accretion rates, close to Eddington. The masses have been inferred from quasar emission line width and continuum luminosity extrapolating empirical relationships established in low redshift active galactic nuclei (AGN) through multi-epoch reverberation mapping. For example, De Rosa et al. (2011) obtain for a population of  $z \sim 6$  quasars a mean black hole mass of  $\log(M_{\text{BH}}/M_{\odot}) \approx 9.06$ , typical bolometric luminosities  $> 10^{47}$  erg s $^{-1}$  and Eddington ratios  $L_{\text{bol}}/L_{\text{Edd}} \approx 0.6$ . The growth time for such black holes and Eddington ratios if starting from  $10^2 M_{\odot}$  seeds is comparable to the age of the Universe at  $z \sim 6$  ( $\sim 0.9$  Gyr). The quasar emission lines also suggest well-developed metallicities. The relative abundance of Fe and  $\alpha$  elements, inferred from Fe II and Mg II emission lines, appears similar to quasars at redshift  $\sim 4$  (e.g. Jiang et al. 2007; De Rosa et al. 2011).

With the advent of ALMA it is now possible to obtain constraints on host dynamical masses and on star formation by observing the cool molecular gas of the hosts. The quasar hosts appear smaller or at most roughly consistent with the present-day relation between host mass and SMBH mass (e.g. Walter et al. 2004, 2009; Wang et al. 2010, 2013; Willott, Bergeron & Omont 2015). These dynamical masses are based on line kinematics. Direct detection of the stellar hosts requires higher spatial resolution and has to await the *James Webb Space Telescope* and the next generation ground-based 30 m-class telescopes (see e.g. Mechtley et al. 2012). The star formation rates measured in the quasar host galaxies are tens to hundred solar masses per year (e.g. Wang et al. 2008, 2013; Walter et al. 2009; Venemans et al. 2012).

The results listed above are mostly based on the brightest (‘tip of the iceberg’) of the quasar population. The quasars have been selected close to the detection limit of flux-limited surveys and represent the bright end of a more common fainter population. They were detectable thanks to the combination of high SMBH mass with high accretion rates. The few notable exceptions are the  $\sim 10^8 M_{\odot}$  SMBHs found by Willott et al. (2010a) and Kashikawa et al. (2015).

Given the steepness of the quasar luminosity function

(see e.g. Fig. 4; Willott et al. 2010b; Kashikawa et al. 2015), a 2.5 mag (a factor 10 in continuum flux density) deeper photometric selection would open the door to a quasar population which is expected to be an order of magnitude more abundant. For a given accretion rate (black hole mass) this population would probe active galaxies with an order of magnitude lower black hole mass (accretion rate).

The abundance of SMBHs at lower masses and accretion rates is a valuable constraint for the various alternative theories for the formation and early evolution of SMBHs and their hosts. These include the remnants of Population III stars, yielding black hole seeds of the order of  $10^2 M_{\odot}$ , direct collapse of primordial dense gas in protogalaxies leading to masses of the order of  $10^{4-5} M_{\odot}$  and run-away dynamical instabilities in dense stellar systems which could result in initial black hole masses of the order of  $10^{2-3} M_{\odot}$  (see e.g. Volonteri 2010, for a review). The theories predict average mass densities for SMBHs seeds at  $z \gg 6$  that differ by up to an order of magnitude. Hydrodynamical simulations are being used to explore in detail these different formation channels. They are now able to predict the relative abundance of bright and faint quasars (e.g. Costa et al. 2014; Katz, Sijacki & Haehnelt 2015; Latif et al. 2015). Thus establishing the quasar demography (accretion rates, star formation rates, host masses) for  $\sim 10^8 M_{\odot}$  SMBHs provides a direct discriminant on the simulated formation scenarios.

The demography of quasars with  $\sim 10^8 M_{\odot}$  SMBH masses is also important for a fair comparison between the SMBH–host galaxy relations at high redshift and today. For today’s SMBH–host relations, selecting black holes which are 10 times lower in mass corresponds to probing stellar hosts which are 10–100 times more abundant, are  $\sim 2$  mag fainter and have  $\sim 35\%$  lower stellar velocity dispersions. At black hole masses of  $10^8 M_{\odot}$  we are also not hampered anymore by the potentially severe selection bias in comparing AGN-selected samples at high redshift to host-selected samples at low redshift. It could be that current high-redshift samples are overwhelmed by exceptionally massive  $10^9 M_{\odot}$  BHs in the more common smaller hosts compared to the much rarer massive galaxies with equally massive black holes (e.g. Willott et al. 2005; Lauer et al. 2007).

For these reasons we are building up a homogeneous sample of faint quasars at  $z \sim 6$  by combining ESO’s public surveys the Kilo Degree Survey (KiDS) and the VISTA Kilo-Degree Infrared Galaxy (VIKING) survey which cover the same area (Arnaboldi et al. 2007; De Jong et al. 2013). The nine-band  $u$  through  $K_s$  photometry from the combined surveys goes up to  $\sim 2$  mag deeper than SDSS, UKIDSS and Pan-STARRS1. Here we report on the high- $z$  quasar harvest from the first year of operations: four quasars in range  $5.8 < z < 6.0$ . The results suggest we can expect to build up a homogeneous sample of the order of 30 faint quasars at  $z \sim 6$ .

This paper is organized as follows. In Section 2, we present the survey data from KiDS and VIKING we made use of and their calibration. The selection of quasar candidates is detailed in Section 3.1, followed by a description of the imaging and spectroscopic follow-up in Sections 3.2 & 3.3. The newly discovered quasars are presented in Section 4 and we conclude with a discussion and outlook in Section 5.

In this paper, we adopt a cosmology with  $\Omega_{\text{M}} = 0.28$ ,

$\Omega_\Lambda = 0.72$  and  $H_0 = 70 \text{ km s}^{-1} \text{ Mpc}^{-1}$  (Komatsu et al. 2011). All magnitudes are given in the AB system.

## 2 KIDS AND VIKING SURVEYS AND DATA

KiDS and VIKING are sister surveys that cover the same  $1500 \text{ deg}^2$  on the sky (Arnaboldi et al. 2007; De Jong et al. 2013). The survey areas are divided over two main strips located in the Northern and Southern Galactic Cap (NGP and SGP). The two strips, roughly equal in area, span  $\sim 10^\circ$  in declination centred on  $(\alpha, \delta) = (12.5\text{h}, 0^\circ)$  and  $(\alpha, \delta) = (0.8\text{h}, -30^\circ)$ . A smaller strip is centred on the GAMA09 region with  $(\alpha, \delta) = (9\text{h}, 0^\circ)$ . KiDS covers the optical Sloan  $u$ ,  $g$ ,  $r$  and  $i$  bands using the OmegaCAM wide-field imager (Kuijken 2011) on the VLT Survey Telescope (VST) at ESO's Paranal Observatory. VIKING covers the near-infrared  $Z$  (hereafter  $Z_V$ ),  $Y$ ,  $J$ ,  $H$  and  $K_s$  using the VISTA InfraRed CAMera (VIRCAM; Dalton et al. 2006) at the VISTA telescope (Emerson, McPherson & Sutherland 2006) also at Paranal. VIKING and KiDS started regular survey operations on 2010 February 15 and 2011 October 15, respectively. The exposure times and depth of the filters used in these two surveys are summarized in Table 1.

In this paper we focus on a set of 267 KiDS  $i$  band slightly overlapping pointings, each with an  $\sim 1.15 \text{ deg}^2$  field of view. They were observed between the nights of 2011 September 2 and 2012 June 7, mostly during bright Moon. Due to slightly different areal scheduling of KiDS and VIKING, the total area with  $i$ ,  $Z_V$  and  $Y$  band coverage was  $254.3 \text{ deg}^2$  with  $96.1 \text{ deg}^2$  covered in the NGP,  $93.2 \text{ deg}^2$  in the SGP and  $65.0 \text{ deg}^2$  was covered in GAMA09. The search for high redshift quasars in this early phase of KiDS operations was approached as a pilot project for the KiDS QSO team. Its aim was to verify the observational quality (in terms of photometry, astrometry, artefacts, data foibles) for quasar candidate selection and the turn-around time between observation and final confirmation via follow-up spectroscopy. We created preliminary  $i$  band calibrated imaging and catalogues using the generic wide-field imaging pipeline in the Astro-WISE<sup>1</sup> survey handling system (McFarland et al. 2013), as operated at OmegaCEN<sup>2</sup>. The processing steps applied to the KiDS  $i$  band data involved:

- removing instrumental fingerprint: de-biasing, flatfielding, preliminary illumination correction and de-fringing,
- primitive flagging/masking for pixels affected by saturation, cosmic rays and satellite tracks,
- preliminary photometric calibration (nightly zero-points) and astrometric calibration (per-chip in a single exposure),
- swarping and coadditions of the five dithers.

The source extraction was performed using SEXTRACTOR (Bertin & Arnouts 1996) configured for point source photometry. The KiDS pointings have overlap with the first public release of the Kilo-Degree Survey

**Table 1.** KiDS and VIKING filters, observing time, nominal depth and typical seeing conditions.

Filter	$\lambda_c$ (Å)	Exposure time (s)	Mag limit (AB $5\sigma$ 2 arcsec)	Seeing (arcsec)
$u$	3550	1000	24.2	1.0
$g$	4775	900	25.1	0.8
$r$	6230	1800	24.9	0.7
$i$	7630	1200	23.5	0.8
$Z_V$	8770	480	22.7	1.0
$Y$	10200	400	22.0	1.0
$J$	12520	400	21.8	0.9
$H$	16450	300	21.1	1.0
$K_s$	21470	480	21.2	0.9

(De Jong et al. 2015). However, the calibration used here predates the calibration of the public release.

For VIKING data we used the images and catalogues processed with the VISTA Data Flow System (Lewis et al. 2005; Lewis, Irwin & Bunclark 2010) by the Cambridge Survey Unit (CASU). Catalogues were also retrieved from the VISTA Science Archive of the Wide-field Astronomy Unit. At the time of our analysis, we could make use of VIKING data produced by the v1.1/1.2 CASU-VIKING pipeline ('CASUVERS=1.1/1.2'). We refer the reader to Venemans et al. (2013) for a description of VIKING and the data products used for the selection of quasar candidates.

## 3 PHOTOMETRIC SELECTION FOR $5.8 < Z < 6.5$ QUASAR CANDIDATES AND FOLLOW-UP OBSERVATIONS

### 3.1 Candidate selection

The selection of candidate quasars at  $z \gtrsim 5.8$  was done as follows. First, the KiDS  $i$  band catalogues were matched with the VIKING  $Z_V Y J H K_s$  catalogues. VIKING sources that had no match in the KiDS catalogues within a 2 arcsec radius were marked as undetected in the  $i$  band and a  $3\sigma$  limiting magnitude appropriate for that corresponding KiDS image was set. The median  $3\sigma$  limiting magnitude of the KiDS data we analysed was 24.0. Redshift  $\sim 6$  quasar candidates were selected in the  $Z_V$  band with a signal-to-noise ratio  $S/N > 7$  and were required to be point sources. Point sources were identified as objects with a galaxy probability  $P_{\text{gal}} < 0.95$  (see Venemans et al. 2013 for a discussion on the efficiency to select point source with  $P_{\text{gal}} < 0.95$ ). To avoid spurious sources with only a detection in the  $Z_V$  band, we further required that an object was also present in the  $Y$  band catalogue. We subsequently applied the following colour criteria to select quasars in the redshift range  $5.8 < z < 6.4$ :

$$i - Z_V > 2.2, Z_V - Y < 1.0 \text{ and } -0.5 < Y - J < 0.5.$$

These colour criteria are based on the work by e.g. Fan et al. (2001) and Venemans et al. (2007) and are illustrated in Fig. 1. In short, quasars at  $z \gtrsim 5.8$  can be identified as objects that drop-out in the  $i$  band. The constraint on the  $Y - J$  colour selects against cool, red stars that can be very faint in  $i$ .

The selection criteria were applied to data obtained

<sup>1</sup> Astronomical Wide-field Imaging System for Europe, <http://www.astro-wise.org>.

<sup>2</sup> OmegaCEN expertise centre for wide-field imaging, <http://www.astro.rug.nl/~omegacen>.

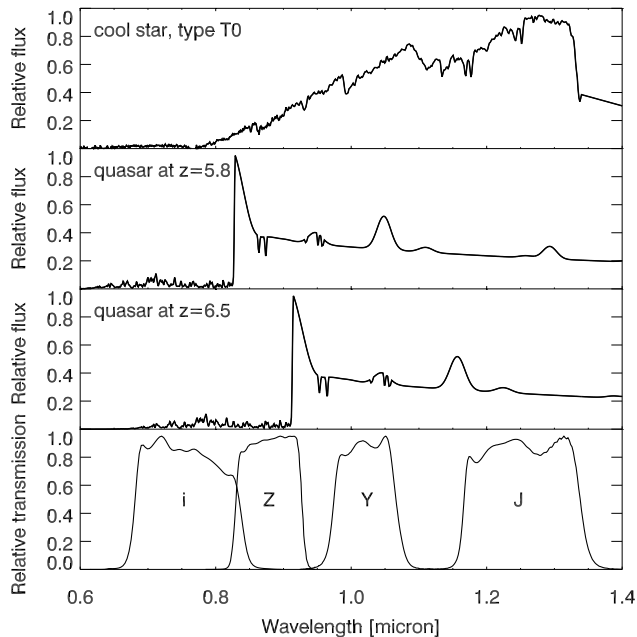


**Figure 1.** The VIKING and KiDS filters used for the quasar search presented here plotted together with a (model) high-redshift quasar at  $z = 5.8$ , a quasar at  $z = 6.5$  and one of the main contaminants, a cool late-type star (data taken from Geballe et al. 2002). Above a redshift of  $z \sim 5.8$ , the Lyman  $\alpha$  line of the quasar shifts out of the  $i$  band, which results in a large measured  $i - Z_V$  colour. Above approximately  $z \sim 6.5$  the Lyman  $\alpha$  line falls outside the  $Z_V$  band filter. Although both high-redshift quasars and cool stars are very faint in the optical  $i$  band, the cool stars generally have a much redder  $Y - J$  colour as compared to quasars.

in three areas NGP, SGP and GAMA09. The NGP and GAMA09 area are also covered by the SDSS. Where SDSS data were available, we applied additional colour criteria, based on the SDSS  $u$  ( $u_s$ ), SDSS  $g$  ( $g_s$ ) and SDSS  $i$  ( $i_s$ ) catalogues. These additional criteria are:

( $i_s - Z_V > 2.2$  OR undetected in  $i_s$ ) and undetected in  $u_s$ ,  $g_s$ ,

where undetected was defined as having a measured magnitude fainter than the  $3\sigma$  limiting magnitude in that band ( $\text{mag} > \text{mag}_{3\sigma}$ ).

Due to the incompleteness of the KiDS  $i$  band catalogues, especially at fainter magnitudes, and to objects close to the edge of the KiDS images, initially our selection criteria returned an unrealistically large number (several thousands) of potential  $z \sim 6$  quasars. In the NGP and GAMA09 region, the inclusion of the SDSS data significantly reduced the number of candidates, especially the number of candidates that were close to the edge of KiDS images. For remaining candidates in those areas and those in the SGP area postage stamps in the  $i$ -band were made in order to reaffirm the magnitude of the sources.

The postage stamps were analysed by measuring the flux of the candidates in an aperture centred on the VIKING position of the candidates. If a flux was measured with an  $S/N > 3$ , and the resulting colour was  $i - Z_V < 2.2$  the object was rejected as high-redshift quasar candidate. The remaining objects were visually inspected to confirm the re-

ality of the candidate. A fraction was located at the edge, or just outside the KiDS imaging area and was removed from the list. We discovered several types of sources that mimic the colours of high-redshift quasars in our setup. Objects moving between the epoch of the VIKING observations and KiDS observations and highly variable objects can have colours that are both blue in the near-infrared bands and very red in  $i - Z_V$ . We were able to remove the majority of these objects as quasar candidates by carefully looking at the VIKING data, which are normally taken in different nights. Images in  $Z_V$ ,  $Y$  and  $J$  are generally taken in grey time, while images in  $J$ ,  $H$  and  $K_s$  are taken during bright time. By comparing the two different  $J$  band epochs and rejecting objects with extremely blue  $Y - K_s$  colours ( $Y - K_s < -0.2$ , while quasars at  $5.8 < z < 6.5$  have  $0.2 < Y - K_s < 0.5$ , e.g. Hewett et al. 2006) we could remove most of the moving and variable objects from our list.

In total, our final candidate list contained 30 sources: 6 objects in the SGP region, 7 objects in the GAMA09 region and 17 candidates in the NGP region.

### 3.2 Follow-up optical imaging

We took images of 29 of our 30  $z \sim 6$  quasar candidates during four separate observing runs. The first run was on 2012 June 29–30 at the 3.58 m ESO New Technology Telescope (NTT) using the European Southern Observatory’s Faint Object Spectrograph and Camera 2 (EFOSC2; Buzzoni et al. 1984). We observed in the filters Gunn  $i$  (filter  $i$  no. 705, hereafter  $I_N$ ) and Gunn  $z$  (filter  $z$  no. 623, hereafter  $Z_N$ ). The second observing run was also with NTT/EFOSC2 on 2012 July 23–25. Thirdly, two candidates were observed with ACAM (Benn, Dee & Agócs 2008) on the William Herschel Telescope (WHT) on 2012 November 10 in service mode, using the filters  $i$  and  $z$ . Finally, we used the NTT again on 2013 March 13–15 to follow-up candidates with EFOSC2.

The candidates were observed with total exposure times between 720 and 2880 s. The integration time for each individual target depended on the sky transparency, seeing and expected brightness of the source. Data reduction steps included bias subtraction, flat fielding using sky flats and sky subtraction using the unregistered science frames. The images were calibrated using bright, unsaturated point sources within the field of view. Since the ACAM  $i$  filter is very similar to the VST  $i$  band, the zero-point of the ACAM  $i$  images were directly derived from the KiDS magnitudes of point sources in the field. The zero-points of the NTT images were computed using relations between  $I_N$  and  $Z_N$  and SDSS and VIKING bands derived from synthesized colours of stars (Venemans et al. 2013). The results of the follow-up photometry are listed in Table 2.

The follow-up imaging rejected 26 of the 29 observed targets as potential  $z \sim 6$  quasars. The majority of rejected candidates have colours consistent with M dwarfs, see Fig. 2. The four objects that remained good quasar candidates were J083955.36+001554.2 (hereafter J0839+0015), J114833.18+005642.3 (hereafter J1148+0056), J121516.88+002324.7 (hereafter J1215+0023) and J032835.51–325322.8 (hereafter J0328–3253). Note that for J0839+0015 we did not obtain any follow-up photometry

**Table 2.** Followup photometry of 29 candidate  $z \sim 6$  quasars in the KiDS+VIKING catalogues. All magnitudes are in AB and limiting magnitudes are  $3\sigma$  limits.

Object name	Filter	Magnitude	Telescope
J020935.59–323206.5	$I_N$	>24.62	NTT
	$Z_N$	>22.83	NTT
J032835.51–325322.8	$I_N$	$21.14 \pm 0.02$	NTT
	$i$	$24.36 \pm 0.45$	WHT
J083635.31–000347.9	$z$	$22.51 \pm 0.21$	WHT
	$z$	$22.94 \pm 0.28$	WHT
J084810.50+021948.2	$i$	$23.08 \pm 0.10$	WHT
	$z$	$22.94 \pm 0.28$	WHT
J090647.34–004216.0	$I_N$	$23.46 \pm 0.43$	NTT
J091026.91–011137.2	$I_N$	$22.24 \pm 0.03$	NTT
J091131.58–001305.5	$I_N$	$23.08 \pm 0.10$	NTT
J092251.90+003245.3	$I_N$	$22.75 \pm 0.05$	NTT
J113549.91+015924.4	$I_N$	$23.07 \pm 0.07$	NTT
	$I_N$	$22.67 \pm 0.05$	NTT
J114833.18+005642.3	$Z_N$	$21.46 \pm 0.15$	NTT
	$I_N$	$23.20 \pm 0.06$	NTT
J121144.38+005348.8	$I_N$	$23.46 \pm 0.08$	NTT
J121404.53+020220.2	$I_N$	$22.38 \pm 0.10$	NTT
J121516.88+002324.7	$I_N$	$22.93 \pm 0.10$	NTT
J122839.49+010253.7	$I_N$	$22.13 \pm 0.02$	NTT
J140552.33+030110.3	$I_N$	$22.65 \pm 0.04$	NTT
J141157.27–001613.5	$I_N$	$22.92 \pm 0.12$	NTT
J142054.44+021247.3	$I_N$	$21.88 \pm 0.02$	NTT
J142300.93+011240.0	$I_N$	$22.53 \pm 0.09$	NTT
J142426.55+011304.1	$I_N$	$22.75 \pm 0.04$	NTT
J143428.30–010043.1	$I_N$	$22.69 \pm 0.03$	NTT
J144130.49+004119.7	$I_N$	$22.52 \pm 0.03$	NTT
J144922.61–004404.9	$I_N$	$22.85 \pm 0.04$	NTT
J145250.27–004047.8	$I_N$	$23.22 \pm 0.05$	NTT
J145442.58–020118.8	$I_N$	$22.59 \pm 0.03$	NTT
J224319.75–331506.8	$I_N$	>23.70	NTT
	$Z_N$	>23.24	NTT
J225656.49–333910.1	$I_N$	$22.10 \pm 0.05$	NTT
J232355.24–303801.7	$I_N$	$22.82 \pm 0.05$	NTT
	$Z_N$	$22.07 \pm 0.12$	NTT
J234331.78–313627.5	$I_N$	$21.30 \pm 0.03$	NTT

(see Section 4.2). For the four remaining objects we took an optical spectrum to confirm their nature.

### 3.3 Spectroscopic observations

The spectroscopic observations of our four remaining quasar candidates were carried out with the FOcal Reducer/low dispersion Spectrograph 2 (FORs2; Appenzeller et al. 1998) on the 8.2 m Very Large Telescope (VLT) Antu. For all observations we used a long slit with a width of 1.3 arcsec and the grism ‘600z’ with a central wavelength of 9010 Å and a resolution of  $R = 1390$ . J0328–3253 was observed on 2012 October 7 for 1782 s in clear conditions with a seeing around 0.8 arcsec. On 2012 December 12 J0839+0015 was observed for 1782 s with a seeing ranging between 1.2 arcsec and 1.7 arcsec. J1215+0023 was observed on 2013 February 7 and 2013 March 5 for a total integration time of 5280 s. The seeing during the February observations varied between 1.4 arcsec and 1.7 arcsec, while in March the conditions were better with a seeing around 0.7 arcsec. Finally, a spectrum of J1148+0056 was taken on 2013 April 13 for 2697 s in a seeing of 0.9 arcsec. All observations were setup in such a

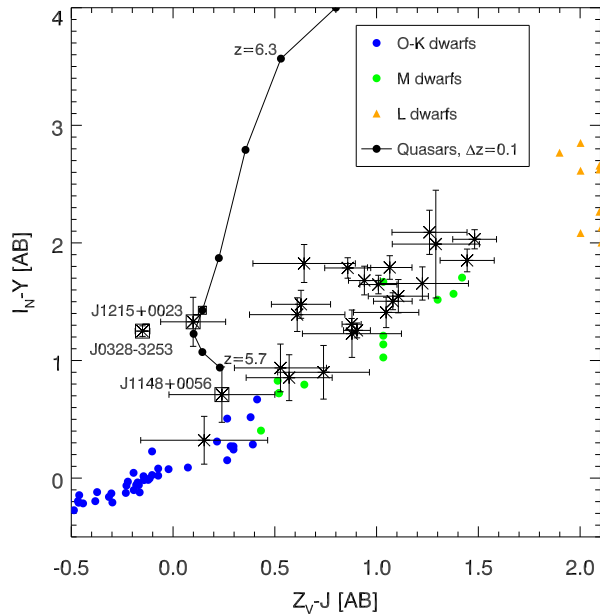


**Figure 2.**  $I_N - Y$  versus  $Z_V - J$  diagram illustrating the outcome of the follow-up NTT imaging of our  $z \sim 6$  quasar candidates. The blue and green circles represent the colours of main sequence stars and M dwarfs, respectively. The yellow triangles are simulated colours of L dwarfs, and the connected black circles illustrate the colours of quasars at various redshifts  $z > 5.7$ . The crosses with error bars represent the candidates observed with the NTT. Based on the  $I_N - Z_V$ ,  $I_N - Z_N$ ,  $I_N - Y$  and  $Z_V - J$  colours most observed candidates were identified as foreground interlopers. The open squares are three objects that remained good candidates after the follow-up imaging and for which we obtained optical spectroscopy (see Section 3.3). Additional  $Z_N$  photometry (see Table 2, not shown in this figure) confirmed that J1148+0056 was a good high-redshift quasar candidate. Note that for a fourth good quasar candidate, J0839+0015, we did not obtain follow-up photometry (see Section 4.2).

way that a nearby bright star was included in the slit to provide a trace for the candidate spectrum.

Daytime exposures of He, Ar and Ne lamps were obtained to provide the wavelength calibration. By measuring the wavelength of sky emission lines in our science spectra we determined that the wavelength calibration had a typical uncertainties between 0.2 and 0.5 Å. For the flux calibration we used observations with a 5 arcsec long slit (taken the same night as the science observations) of one of the spectrophotometric standard stars Feige 110, HD49798, LTT4816 and LTT7379 (Oke 1990; Hamuy et al. 1992, 1994). Finally the flux calibrated spectra were scaled to the VIKING  $Z_V$  band magnitudes to account for slit losses.

The reduced spectra of the four quasar candidates are shown in Fig. 3.

## 4 FOUR QUASARS AROUND A REDSHIFT OF 6

The four targets of our follow-up spectroscopy all show a blue continuum with a sharp break between 8300 and 8500 Å, characteristic of quasars at  $z \sim 6$ . To measure the

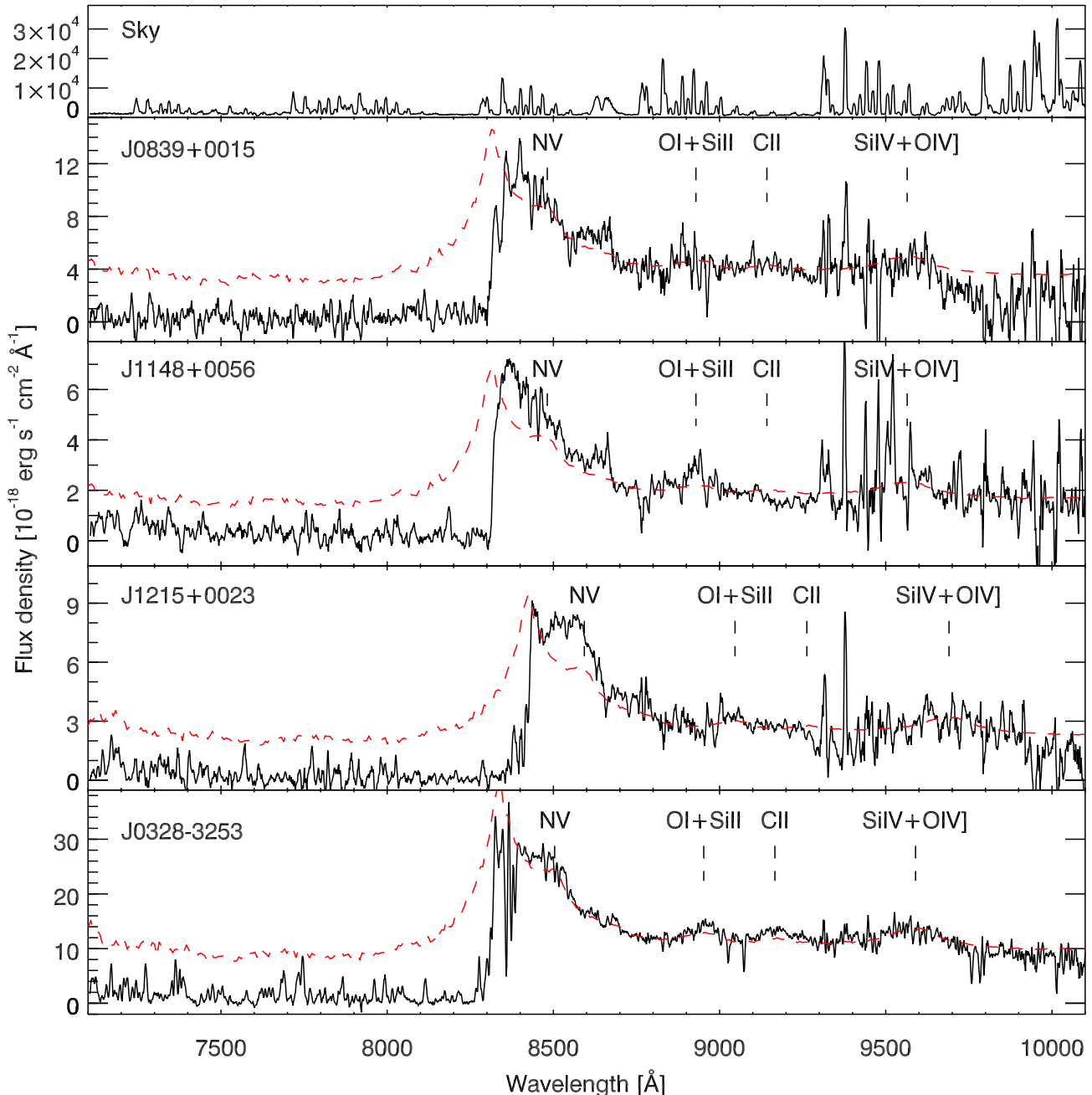


**Figure 3.** Discovery spectra from VLT/FORS2 of three  $z \sim 6$  quasars in the KiDS+VIKING survey. The spectra of J0839+0015 and J1215+0023 are boxcar averaged over five pixels. For comparison, a spectrum of the sky is plotted at the top. The position of several emission lines are marked. The spectra are overplotted with the composite quasar spectrum from Vanden Berk et al. (2001).

redshift of the newly identified quasars, we measured the redshifted position of emission lines in the spectra. When visible, the emission lines we used for this purpose are O I + Si II at  $\lambda_{\text{rest}} = 1305.42 \text{ \AA}$ , C II at  $\lambda_{\text{rest}} = 1336.6 \text{ \AA}$  and Si IV + O IV at  $\lambda_{\text{rest}} = 1398.33 \text{ \AA}$ . The central wavelength of the emission lines are taken from the composite quasar spectrum by Vanden Berk et al. (2001). To compute the absolute magnitudes of the quasars at a rest-frame wavelength of  $1450 \text{ \AA}$  ( $M_{1450}$ ), we fitted a power-law slope in regions without emission lines. The regions used were  $1270 < \lambda_{\text{rest}}/\text{\AA} < 1295$ ,

$1315 < \lambda_{\text{rest}}/\text{\AA} < 1325$  and  $1345 < \lambda_{\text{rest}}/\text{\AA} < 1370$ . Below we describe the new quasars in more detail. A summary of the properties of the quasars is given in Table 3.

#### 4.1 J0328–3253 at $z = 5.86$

This quasar was selected as a high signal-to-noise ratio candidate in our KiDS+VIKING catalogues. This source has a  $Z_V$  band magnitude of  $Z_V = 19.8$  and blue infrared colours of  $Z_V - Y = -0.1$  and  $Y - J = -0.1$  (Table 3).

The source was detected in the  $i$  band with a magnitude of  $i = 22.14 \pm 0.06$  and thus had a  $i - Z_V = 2.3$ . Follow-up photometry with the NTT confirmed a break in the spectral energy distribution of the source shortwards of the  $Z_V$  band. The  $I_N - Z_V = 1.3$ , consistent with a quasar at  $z \sim 5.8$ . VLT/FORS2 spectroscopy confirmed that the source is at  $z = 5.86 \pm 0.03$  (Fig. 3). We measured the redshift using the emission lines O I + Si II, C II and Si IV + O IV] and found a redshift around  $z = 5.86$  for all three lines. Our power-law fit to the continuum gives an absolute magnitude of  $M_{1450} = -26.60 \pm 0.04$ . After our discovery of this quasar in 2012, the object was independently selected as a bright quasar candidate in the VST-ATLAS survey (Carnall et al. 2015).

#### 4.2 J0839+0015 at $z = 5.84$

This object was initially selected with  $i - Z_V > 2.7$ ,  $Z_V - Y = -0.1$  and  $Y - J = 0.3$  (Table 3). Analysis of the  $i$  band postage stamp revealed a faint source with a magnitude of  $i = 23.46 \pm 0.33$ , resulting in an  $i - Z_V \sim 2.4$ . The two epochs of near-infrared data did not show strong variability and the detection of a source in the  $i$  band ruled out that this object was moving. We therefore decided to take a spectrum of this source. Despite poor observing conditions the resulting spectrum clearly shows a break at  $\sim 8300 \text{ \AA}$  (Fig. 3). If this break is at the wavelength of Lyman  $\alpha$ , then the redshift would be around  $z \sim 5.83$ . This redshift was confirmed by measuring the position of faint emission lines. The O I + Si II gave a redshift of  $z \sim 5.81$ , while the Si IV + O IV] line gave  $z \sim 5.87$ . We therefore estimate that the redshift of this quasar is  $z = 5.84 \pm 0.04$ . The continuum fit gives an absolute magnitude of  $M_{1450} = -25.36 \pm 0.11$ .

#### 4.3 J1148+0056 at $z = 5.84$

The source J1148+0056 was selected as a faint ( $Z_V = 21.8$ ) candidate with colours  $i - Z_V > 2.3$ ,  $Z_V - Y = -0.2$  and  $Y - J = 0.4$ . The  $i$  band postage stamp showed no source at the position of the  $Z_V$  band object. Follow-up imaging with the NTT measured a colour of  $I_N - Z_N = 1.2$  and  $Z_N - J = -0.3$ , consistent with a high redshift quasar. Optical spectroscopy detected a source with continuum longwards of  $\lambda \sim 8300 \text{ \AA}$  and faint emission lines at  $8930 \text{ \AA}$  and at  $9115 \text{ \AA}$ . We identified these lines with O I + Si II and C II redshifted to  $z = 5.84 \pm 0.03$ . From a power-law fit to the continuum we estimate that the absolute magnitude of this quasar is  $M_{1450} = -24.46 \pm 0.11$ , which makes it the faintest quasar in our sample.

#### 4.4 J1215+0023 at $z = 5.93$

J1215+0023 was a high priority quasar candidate in our lists with colours  $i - Z_V > 2.7$ ,  $Z_V - Y = -0.2$  and  $Y - J = 0.3$ . NTT imaging confirmed that the source had a break in the spectral energy distribution shortwards of the  $Z_V$  band ( $I_N - Z_V = 1.5$ ). From the FORS2 spectrum we measure a redshift of  $z = 5.93 \pm 0.03$ , based on the O I + Si II and Si IV + O IV] lines. From the continuum we measure an absolute magnitude of  $M_{1450} = -24.67 \pm 0.14$ .

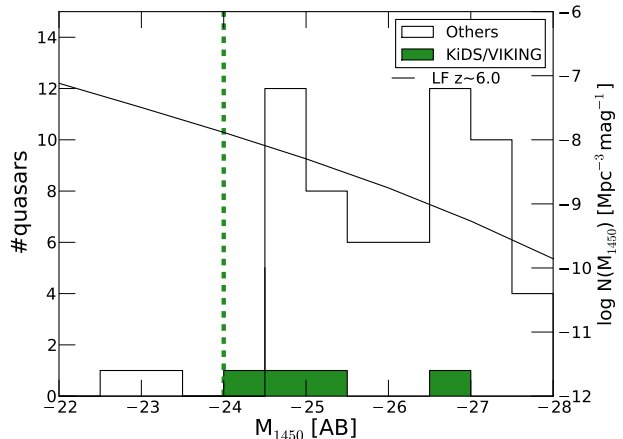


**Figure 4.** Distribution of quasars in the redshift range  $5.8 < z < 6.4$  as function of absolute magnitude. Plotted are the histograms of the 60 previously published quasars in this redshift range (white) and new quasars discovered with the KiDS/VIKING survey pilot (green). The solid black curve indicates the luminosity function for quasars at redshift 6 as derived by Kashikawa et al. (2015), using their ‘case 1’. The dashed green line indicates the selection limit, i.e., the intrinsically faintest quasars that we could select with the KiDS/VIKING survey. The aim of the KiDS/VIKING survey is to triple the number of known quasars fainter than  $M_{1450} > -25$ .

## 5 DISCUSSION AND OUTLOOK

By combining KiDS  $i$  band data with VIKING  $Z_V, Y, J, H, K_s$  catalogues, we performed a pilot study to search for faint  $z \sim 6$  quasar candidates. In our first year of obtaining follow-up data, we discovered four new quasars in an area of  $\sim 254 \text{ deg}^2$ . To compare our quasars with those of other high redshift quasar searches we plot in Fig. 4 the  $z \sim 6$  quasar luminosity function from Kashikawa et al. (2015) as function of absolute magnitude. Overplotted is a histogram of the 60 known quasars at  $5.8 < z < 6.4$ , taken from the literature (Zeimann et al. 2011; Bañados et al. 2014; Calura et al. 2014; Kashikawa et al. 2015; Carnall et al. 2015; Jiang et al. 2015; Reed et al. 2015, and references therein). The new quasars from the KiDS/VIKING surveys are generally fainter ( $Z_V \text{ mag} \gtrsim 21$ ) than the quasars found in, for example, the SDSS and PS1 surveys, showing that our  $z \sim 6$  quasar search is probing the faint end of the known  $z = 6$  quasar population.

One of the questions is how many quasars we were expecting in our survey. To estimate this, we took the  $z \sim 6$  quasar luminosity function and computed the expected number of quasars as function of area and limiting magnitude. The limiting magnitude varied from area to area, and mostly depended on the depth of the KiDS  $i$ -band imaging. The median depth to which we could search for quasars was  $Z_V \sim 21.65$ . We integrated the Willott et al. (2010b) luminosity function<sup>3</sup> and in the redshift range  $5.8 < z < 6.4$

<sup>3</sup> Using the Kashikawa et al. (2015) luminosity function instead of the Willott et al. (2010b) luminosity function gives the same result.

**Table 3.** Properties of the newly discovered quasars. The redshift uncertainty does not include the uncertainty between the redshift of the UV emission lines and the systemic redshift of the quasars. The uncertainty in the absolute magnitude is a combinations of the uncertainty in the continuum fit and in the absolute scaling of the spectrum based on the  $Z_V$ -band magnitude.

Object name	RA (J2000)	Dec. (J2000)	Redshift	$Z_{\text{VIKING}}$	$Y_{\text{VIKING}}$	$J_{\text{VIKING}}$	$K_{s,\text{VIKING}}$	$M_{1450}$
J0328–3253	03 <sup>h</sup> 28 <sup>m</sup> 35 <sup>s</sup> .511	–32°53′22″.92	5.86±0.03	19.83±0.02	19.89±0.04	19.98±0.03	19.69±0.05	–26.60±0.04
J0839+0015	08 <sup>h</sup> 39 <sup>m</sup> 55 <sup>s</sup> .356	+00°15′54″.21	5.84±0.04	21.09±0.05	21.19±0.10	20.89±0.11	20.50±0.15	–25.36±0.11
J1148+0056	11 <sup>h</sup> 48 <sup>m</sup> 33 <sup>s</sup> .180	+00°56′42″.26	5.84±0.03	21.79±0.10	21.96±0.23	21.55±0.24	21.20±0.23	–24.46±0.11
J1215+0023	12 <sup>h</sup> 15 <sup>m</sup> 16 <sup>s</sup> .879	+00°23′24″.74	5.93±0.03	21.42±0.07	21.60±0.18	21.32±0.14	21.10±0.21	–24.67±0.14

we expected  $\sim 7$  quasars in the area we surveyed, where we discovered four. The difference between the predicted number and the observed number of quasars might well be due to various sources of incompleteness of our search. The most prominent ones are: catalogue completeness, point source selection efficiency and completeness of the colour selection. In Venemans et al. (2013) it was found that the VIKING catalogue completeness is  $\sim 96\%$  above a S/N of 7, while the fraction of point sources that is incorrectly classified as extended objects is around 6%–7%. The largest incompleteness is the colour incompleteness: both due to random photometric errors and due to small variations in the quasar spectral energy distribution and in the intergalactic medium (IGM) absorption, quasars can be placed outside our colour selection box. For example, quasars with a redshift around  $z \sim 5.8$  have an  $i - Z_V$  colour that is a steep function of redshift, see e.g. fig. 1 in Bañados et al. (2014). It is therefore possible that we are missing quasars around  $z \sim 5.8$  that have  $i - Z_V < 2.2$ . Indeed, by matching our data with high-redshift quasars that have previously been discovered, we found that the SDSS quasar J0836+0054 at  $z = 5.82$  (Fan et al. 2001) is detected in both the VIKING and KiDS survey. While the redshift of this quasar is very close to the ones we present in this paper, J0836+0054 has an  $i - Z_V = 1.70$ , well below our cut of  $i - Z_V = 2.2$ . At the high end of our probed redshift range,  $z \sim 6.4$ , due to variations in the IGM and in the quasar’s emission line strength and due to photometric uncertainties, quasars can become too red in  $Z_V - Y$  to be selected by our colour criterion ( $Z_V - Y < 1.0$ , see Section 3.1). In Venemans et al. (2013) it was shown through modelling that up to 15% of artificial quasars at  $z = 6.4$  fulfilled the colour selection  $Z_V - Y > 1.1$ . This indicates that we are also incomplete in our selection of quasars at  $z = 6.3 - 6.4$ . Combined with the other sources of incompleteness, the discovery of four new quasars is well in line with the theoretical expectation of seven.

The total area that ultimately will be covered by the KiDS and VIKING surveys is 1500 deg<sup>2</sup>, roughly six times the area we searched in our pilot study. We therefore expect to discover at least 20 additional quasars in this area. Furthermore, there are several ways to push our quasar search to even fainter magnitudes. For example, when selecting quasar candidates, we could reduce the  $i - Z_V$  colour limit to  $i - Z_V = 2.0$  (similar to the PS1 quasar search, see Bañados et al. 2014). This will increase our completeness, especially at the low-redshift end of our quasar search,  $z \sim 5.8$ . Additionally, our requirement for a candidate to have a detection in the  $Y$  band, while significantly reducing the number of spurious sources, limits in certain areas how faint we can select candidates as the  $i$  and  $Z_V$  band cata-

logues are deeper than the  $Y$ -band catalogue (see Table 1). By pushing our selection to fainter magnitudes, we should be able to uncover quasars as faint as  $M_{1450} = -24$ . Based on the quasar luminosity function, we therefore expect to discover at least 30 more quasars down to  $M_{1450} = -24$ , significantly increasing the number of quasars at these faint absolute magnitudes.

Besides exploring the new survey data that will become available, our plan is to characterize the newly discovered quasars with near-infrared, far-infrared and sub-mm spectroscopy. This will allow us to constrain black hole masses, ISM metallicity and host masses. This is important to understand the relationship between the accreting black hole and the stellar component of galaxies in the first billion years of the Universe.

## ACKNOWLEDGEMENTS

The authors are grateful for advice and support by the KiDS Production Team during this early pilot programme in the first year of KiDS operations. This work is financially supported by the Netherlands Research School for Astronomy (NOVA) and Target. Target is supported by Samenwerkingsverband Noord Nederland, European fund for regional development, Dutch Ministry of economic affairs, Pieken in de Delta, Provinces of Groningen and Drenthe. Target operates under the auspices of Sensor Universe. BPV acknowledges funding through the ERC grant ‘Cosmic Dawn’. EB thanks the IMPRS for Astronomy & Cosmic Physics at the University of Heidelberg. This work is supported by the Netherlands Organization for Scientific Research (NWO) through grant 614.061.610 (JdJ). This publication has made use of data from the VIKING survey from VISTA and KiDS survey from the VST at the ESO Paranal Observatory, under programme IDs 179.A-2004, 177.A-3016, 177.A-3017 and 177.A-3018. Data processing has been contributed by the VISTA Data Flow System at CASU, Cambridge and WFAU, Edinburgh and the Astro-WISE Data Flow System at OmegaCEN, Kapteyn Astronomical Institute, University of Groningen. *Author Contributions:* all authors contributed to the development and writing of this paper. The authorship list reflects the lead authors (BV, GVK, JM, EV) followed by two alphabetical groups. The first alphabetical group (EB, RD) includes those who are key contributors to both the scientific analysis and the data products. The second group covers those who have either made a significant contribution to the data products, or to the scientific analysis.

## REFERENCES

- Abazajian K. N. et al., 2009, *ApJS*, 182, 543
- Appenzeller I. et al., 1998, *The Messenger*, 94, 1
- Arnaboldi M., Neeser M. J., Parker L. C., Rosati P., Lombardi M., Dietrich J. P., Hummel W., 2007, *The Messenger*, 127, 28
- Bañados E. et al., 2014, *AJ*, 148, 14
- Benn C., Dee K., Agócs T., 2008, in McLean I. S., Casali M. M., eds, *Proc. SPIE Conf. Ser. Vol. 7014, Ground-based and Airborne Instrumentation for Astronomy II*. SPIE, Bellingham, p. 70146X
- Bertin E., Arnouts S., 1996, *A&AS*, 117, 393
- Buzzoni B. et al., 1984, *The Messenger*, 38, 9
- Calura F., Gilli R., Vignali C., Pozzi F., Pipino A., Matteucci F., 2014, *MNRAS*, 438, 2765
- Carilli C. L., Walter F., 2013, *ARA&A*, 51, 105
- Carnall A. C. et al., 2015, *MNRAS*, 451, L16
- Costa T., Sijacki D., Trenti M., Haehnelt M. G., 2014, *MNRAS*, 439, 2146
- Dalton G. B. et al., 2006, in McLean I. S., Iye M., eds, *Proc. SPIE Conf. Ser. Vol. 6269, Ground-based and Airborne Instrumentation for Astronomy*. SPIE, Bellingham, p. 62690X
- De Jong J. T. A., Verdoes Kleijn G. A., Kuijken K. H., Valentijn E. A., 2013, *Exp. Astron.*, 35, 25
- De Jong J. T. A. et al., 2015, preprint (arXiv:1507.00742)
- De Rosa G., Decarli R., Walter F., Fan X., Jiang L., Kurk J., Pasquali A., Rix H. W., 2011, *ApJ*, 739, 56
- Emerson J., McPherson A., Sutherland W., 2006, *The Messenger*, 126, 41
- Fan X. et al., 2001, *AJ*, 122, 2833
- Fan X. et al., 2006, *AJ*, 132, 117
- Geballe T. R. et al., 2002, *ApJ*, 564, 466
- Hamuy M., Suntzeff N. B., Heathcote S. R., Walker A. R., Gigoux P., Phillips M. M., 1994, *PASP*, 106, 566
- Hamuy M., Walker A. R., Suntzeff N. B., Gigoux P., Heathcote S. R., Phillips M. M., 1992, *PASP*, 104, 533
- Heckman T. M., Kauffmann G., Brinchmann J., Charlot S., Tremonti C., White S. D. M., 2004, *ApJ*, 613, 109
- Hewett P. C., Warren S. J., Leggett S. K., Hodgkin S. T., 2006, *MNRAS*, 367, 454
- Jiang L. et al., 2009, *AJ*, 138, 305
- Jiang L., Fan X., Vestergaard M., Kurk J. D., Walter F., Kelly B. C., Strauss M. A., 2007, *AJ*, 134, 1150
- Jiang L., McGreer I. D., Fan X., Bian F., Cai Z., Clément B., Wang R., Fan Z., 2015, *AJ*, 149, 188
- Kashikawa N. et al., 2015, *ApJ*, 798, 28
- Katz H., Sijacki D., Haehnelt M. G., 2015, *MNRAS*, 451, 2352
- Komatsu E. et al., 2011, *ApJS*, 192, 18
- Kormendy J., Ho L. C., 2013, *ARA&A*, 51, 511
- Kuijken K., 2011, *The Messenger*, 146, 8
- Latif M. A., Bovino S., Grassi T., Schleicher D. R. G., Spaans M., 2015, *MNRAS*, 446, 3163
- Lauer T. R., Tremaine S., Richstone D., Faber S. M., 2007, *ApJ*, 670, 249
- Lawrence A. et al., 2007, *MNRAS*, 379, 1599
- Lewis J. R., Irwin M., Bunclark P., 2010, in Mizumoto Y., Morita K.-I., Ohishi M., eds, *ASP Conf. Ser. Vol. 434, Astronomical Data Analysis Software and Systems XIX*. Astron. Soc. Pac., San Francisco, p. 91
- Lewis J. R., Irwin M. J., Hodgkin S. T., Bunclark P. S., Evans D. W., McMahon R. G., 2005, in Shopbell P., Britton M., Ebert R., eds, *ASP Conf. Ser. Vol. 347, Astronomical Data Analysis Software and Systems XIV*. Astron. Soc. Pac., San Francisco, p. 599
- Madau P., Dickinson M., 2014, *ARA&A*, 52, 415
- McFarland J. P., Verdoes-Kleijn G., Sikkema G., Helmich E. M., Boxhoorn D. R., Valentijn E. A., 2013, *Exp. Astron.*, 35, 45
- Mechtley M. et al., 2012, *ApJL*, 756, L38
- Morganson E. et al., 2012, *AJ*, 143, 142
- Mortlock D. J. et al., 2011, *Nature*, 474, 616
- Oke J. B., 1990, *AJ*, 99, 1621
- Reed S. L. et al., 2015, preprint (arXiv:1504.03264)
- Vanden Berk D. E. et al., 2001, *AJ*, 122, 549
- Venemans B. P. et al., 2015, *ApJL*, 801, L11
- Venemans B. P. et al., 2013, *ApJ*, 779, 24
- Venemans B. P. et al., 2012, *ApJL*, 751, L25
- Venemans B. P., McMahon R. G., Warren S. J., Gonzalez-Solares E. A., Hewett P. C., Mortlock D. J., Dye S., Sharp R. G., 2007, *MNRAS*, 376, L76
- Volonteri M., 2010, *A&AR*, 18, 279
- Walter F., Carilli C., Bertoldi F., Menten K., Cox P., Lo K. Y., Fan X., Strauss M. A., 2004, *ApJ*, 615, L17
- Walter F., Riechers D., Cox P., Neri R., Carilli C., Bertoldi F., Weiss A., Maiolino R., 2009, *Nature*, 457, 699
- Wang R. et al., 2010, *ApJ*, 714, 699
- Wang R. et al., 2008, *ApJ*, 687, 848
- Wang R. et al., 2013, *ApJ*, 773, 44
- Willott C. J. et al., 2010a, *AJ*, 140, 546
- Willott C. J., Bergeron J., Omont A., 2015, *ApJ*, 801, 123
- Willott C. J. et al., 2010b, *AJ*, 139, 906
- Willott C. J., Percival W. J., McLure R. J., Crampton D., Hutchings J. B., Jarvis M. J., Sawicki M., Simard L., 2005, *ApJ*, 626, 657
- Zeimann G. R., White R. L., Becker R. H., Hodge J. A., Stanford S. A., Richards G. T., 2011, *ApJ*, 736, 57